Eur. Phys. J. B **18**, 413–419 (2000)

THE EUROPEAN PHYSICAL JOURNAL B

EDP Sciences

Effect of the structural quality of the buffer on the magnetoresistance and the exchange coupling in sputtered Co/Cu sandwiches

A. Dinia[1,a], N. Persat[1], S. Colis[1], C. Ulhaq-Bouillet[1], and H.A.M. van den Berg[2]

[1] IPCMS-GEMME[b], ULP-ECPM, 23 rue du Loess, 67037 Strasbourg Cedex, France
[2] Siemens AG, ZT MF 1, Paul Gossenstrasse 100, 91052 Erlangen, Germany

Received 11 July 2000

Abstract. The effect of the structural quality of the buffer stack on the structural properties, giant magnetoresistance (GMR) and the quality of the antiferromagnetic coupling has been investigated for Co/Cu/Co sandwiches prepared by DC-magnetron sputtering. Three kinds of buffers were employed: type A: Cr(6 nm)/Co(0.8 nm)/Cu(10 nm), type B: Fe(6 nm)/Co(0.8 nm)/Cu(10 nm) and type C: Cr(4 nm)/Fe(3 nm)/Co(0.8 nm)/Cu(10 nm). For B and C type buffers, the antiferromagnetic alignment is very interesting at zero field with a coupling strength larger than 0.4 erg/cm^2 and a GMR signal reaching 5% at room temperature. However, for the A type buffer the antiferromagnetic coupling completely disappears, while the GMR drops to about 0.8%. X-ray diffraction, atomic force microscopy and transmission electron microscopy have been performed in order to understand the origin of the observed difference in the magnetic properties. The results show a strong difference in the average surface roughness, 1.15 nm and 0.35 nm, respectively for the A and C types buffers, and demonstrate that the quality of the surface of the buffer is the key to optimize both the GMR and the indirect exchange coupling.

PACS. 75.70.-i Magnetic films and multilayers – 75.70.Cn Interfacial magnetic properties (multilayers, magnetic quantum wells, superlattices, magnetic heterostructures) – 75.70.Pa Giant magnetoresistance

1 Introduction

In the past decade, improved sample preparation techniques have made it possible to study magnetic multilayer systems of unprecedented quality, revealing new physical properties. In particular, the antiferromagnetic (AF) exchange coupling [1] between ferromagnetic layers separated by a nonmagnetic metallic spacer layer with certain specific thicknesses as well as giant magnetoresistance (GMR) [2].

The Co/Cu multilayers have been studied widely. It has been reported that polycristalline Co/Cu multilayers with (111) texture prepared by sputtering exhibit antiferromagnetic exchange coupling and a GMR that can reach 65% at room temperature [3,4]. In contrast, unless special techniques are used, single-crystal superlattices grown by molecular beam epitaxy (MBE) very often fail to yield a GMR at all [5]. This apparent anomaly was clarified when the first observation of GMR in (111)Co/Cu superlattices grown by MBE was reported [6]. A large variety of results on antiferromagnetic coupling and GMR in Co/Cu system [7–11] has been reported for thin films prepared by the same technique, AF coupling strength (J_{AF}) which vary from 0.3 erg/cm^2 [12] to 0.45 erg/cm^2 [13] oscillation periods between 1 [3] to 1.3 nm [14] and GMR values between 51% [15] and 80% [3,16]. Such a dispersion in the results for the same system, prepared by the same technique, demonstrates clearly how sensitive to the preparation conditions the magnetic and the transport properties are.

In order to obtain a perfect antiferromagnetic coupling (which means 100% antiparallel alignment of the adjacent Co layers through the Cu nonmagnetic layer), some effort has to be put into the samples preparation and the choice of the buffer layer. This can lead to a general improvement in structured quality by reducing structural defects such as surface roughness, direct contact between the magnetic layers etc. which may lead to direct or ferromagnetic coupling instead of the desired antiferromagnetic coupling.

This is exactly what has been done in this study, which aims to show that the choice of an adequate buffer layer makes it possible to obtain nearly perfect AF coupling with complete AF alignment with a negligible amount of remanent magnetization for a Co/Cu sandwich prepared by sputtering. Firstly, magnetoresistance curves are presented in order to demonstrate the quality of the AF coupling. As the GMR is very sensitive to structural defects,

[a] e-mail: aziz@ipcms.u-strasbg.fr
[b] UMR 7504 du CNRS

the shape of this signal is a good indicator of growth quality. Then, X-ray diffraction, atomic force microscopy, and transmission electron microscopy analysis are reported to explain the origin of the optimized antiferromagnetic coupling and GMR.

2 Experimental details

The sandwiches have been prepared by DC-magnetron sputtering with a base pressure of 5×10^{-8} mbar and deposited on glass or silicon substrates at room temperature. The sandwiches consist of Co(1.2 nm)/Cu(t_{Cu})/Co(1.2 nm) with $t_{\mathrm{Cu}} = 0.83$ nm near the first AF peak in the oscillatory interlayer coupling. Three types of buffers were employed [14]: type A: Cr(6 nm)/Co(0.8 nm)/Cu(10 nm), type B: Fe(6 nm)/Co(0.8 nm)/Cu(10 nm) and type C: Cr(4 nm)/Fe(3 nm)/Co(0.8 nm)/Cu(10 nm). The purpose of the 10 nm thick Cu layer is to exchange decouple the Co/Cu/Co sandwich from the magnetic part of the buffer stack, and, in addition, to provide a smooth surface for the growth of the Co/Cu/Co sandwich. The samples were protected by a Cu(2 nm)/Cr(2 nm) capping layer.

The GMR curves were measured at room temperature by the standard four-point method with orthogonal sensing current and applied magnetic field in the plane of the layers. Magnetization curves have been measured using an alternating gradient force magnetometer (AGFM) with the magnetic field applied in the film plane.

The X-ray measurements were performed at room temperature using a Siemens powder diffractometer with monochromatic Cu or Co K_{α_1} radiation. The geometry of the diffractometer allows only experiments in reflection mode.

The surface roughness was studied by analyzing many different line scans with various lengths using an Atomic Force Microscope. The roughness distribution on the surface of the samples is well fitted by a Gaussian function described by its root mean square (RMS).

TEM observations were performed at Strasbourg with a high resolution electron microscope TOPCON EM002B operating at 200 kV with point to point resolution of 0.18 nm at Scherzer defocus. While at Munich a Philips TM 200 FEG electron microscope has been used which is equipped with field emission gun and operating at 200 kV providing a resolution of 0.2 nm. The spatial resolution for the diffraction patterns was better than 10 to 20 nm. Only samples deposited on silicon substrates have been prepared for TEM plan-view and cross-section observations, either by an ionless tripod technique [17] or by ion milling at liquid nitrogen temperature.

3 Magneto-transport properties

The use of a Fe buffer layer is known to lead to a strong and complete antiferromagnetic coupling in sputtered Co/Cu multilayers, which consequently exhibit high magnetoresistance ratio for multilayers with a large number of periods [3]. This is, however, hard to achieve for a single period stack. The Co(1.2 nm)/Cu(0.83 nm)/Co(1.2 nm) sandwich has been grown on the following buffer: Fe(6 nm)/Co(0.8 nm)/Cu(10 nm). The GMR curves are reported in Figure 1. It is clearly seen that both GMR and AF coupling are very interesting. The GMR value is around 6%, which is relatively high for a sandwich stack. There are only a few previous studies on GMR in Co/Cu sandwiches [11,14] and these report lower GMR values than the 6% observed in our case. This is a first indication of the high quality of our samples. Using the saturation field value H_{S}, the saturation magnetization of bulk Co, M_{S} (since in this case the presence of a 6 nm thick Fe buffer layer makes the determination of the magnetization saturation of the Co very difficult) and the following expression: $J_{\mathrm{AF}} = H_{\mathrm{S}} M_{\mathrm{S}} t_{\mathrm{Co}}/2$, where t_{Co} is the ferromagnetic thickness of the Co layer and the factor 2 explains that only two surfaces are involved in the exchange coupling, we found $J_{\mathrm{AF}} = 0.43$ erg/cm^2. This value is among the highest values observed in sputtered or in MBE grown Co/Cu systems. A large GMR and exchange coupling strength do not guarantee that the antiferromagnetic coupling is complete. This is made, however, difficult since the analysis of the magnetization curve is hampered by the thick Fe layer and particularly in the case of a sandwich containing two very thin Co layers [14]. As a consequence, the estimation of the amount of the remanent magnetization in the Co/Cu/Co system itself is made difficult. Although the magnetic signal of the Fe layer can in principle be easily evaluated separately, difficulties are encountered when subtracting from the total magnetization, the signal of the separately grown Fe layer. This arises from the fact that the signal of this layer, in particular its coercivity, is affected by the stack grown on top of it.

Therefore, we attempted to replace the magnetic layer by a nonmagnetic one. A Cu buffer layer is known to induce rough interfaces in Co/Cu systems [3]. Cr exhibits

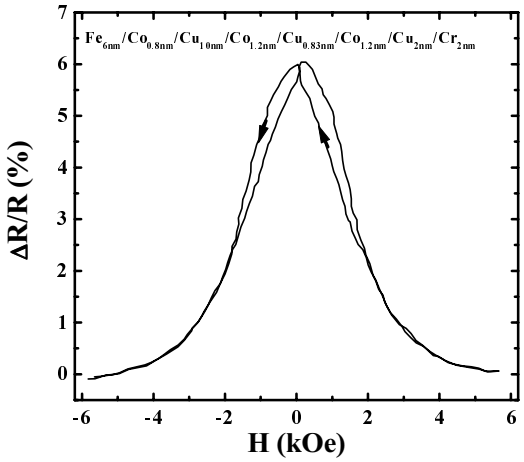

Fig. 1. Magnetoresistance curves measured at room temperature with the magnetic field in the film plane and parallel to the current direction for the following sandwich: Fe(6 nm)/Co(0.8 nm)/Cu(10 nm)/Co(1.2 nm)/Cu(0.83 nm)/Co(1.2 nm)/Cu(2 nm)/Cr(2 nm).

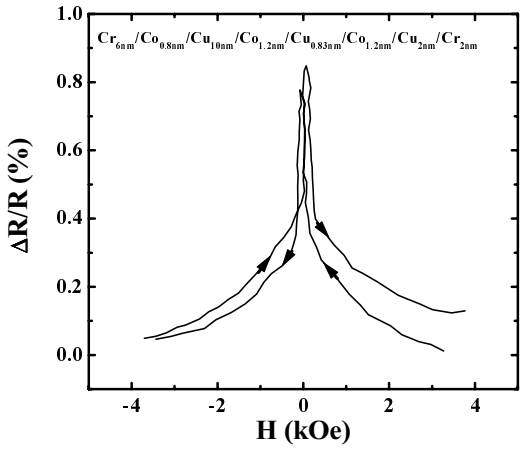

Fig. 2. Magnetoresistance curves measured at room temperature with the magnetic field in the film plane and parallel to the current direction for the following sandwich: Cr(6 nm)/Co(0.8 nm)/Cu(10 nm)/Co(1.2 nm)/Cu(0.83 nm)/Co(1.2 nm/Cu(2 nm)/Cr(2 nm).

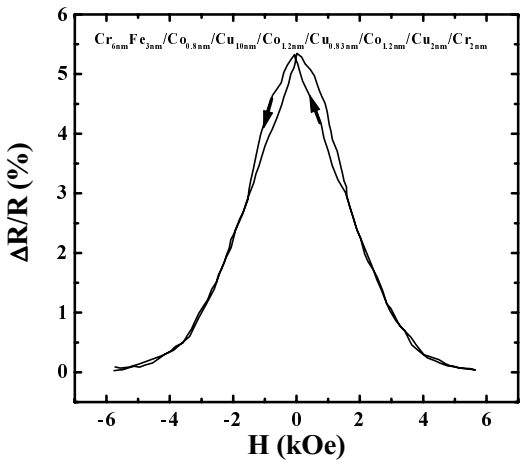

Fig. 3. Magnetoresistance curves measured at room temperature with the magnetic field in the film plane and parallel to the current direction for the following sandwich: Cr(4 nm)/Fe(3 nm)/Co(0.8 nm)/Cu(10 nm)/Co(1.2 nm)/Cu(0.83 nm)/Co(1.2 nm)/Cu(2 nm)/Cr(2 nm).

much crystallographic resemblance to Fe and has high affinity to the oxygen of the glass substrate. The Cr(6 nm)/Co(0.8 nm)/Cu(10 nm) buffer has been used for the artificial antiferromagnetic subsystem (AAF) growth. The results reported in Figure 2, show unfortunately that the AF coupling vanishes completely and the GMR drops to 0.8%. This effect is attributed to the roughness as will be evidenced later by transmission electron microscopy.

In order to reduce the magnetic contribution of the buffer layer and to optimize the GMR and the exchange coupling, we have decided to use both Fe and Cr in the buffer layer. Several combinations have been made and the best results have been obtained with a tiny Fe layer (3 nm) between a 4 nm Cr layer and 10 nm Cu layer. This buffer makes it possible to re-establish both the antiferromagnetic coupling and the GMR. As shown in Figure 3, the GMR and the interlayer coupling strength are close to the values obtained with the Fe buffer. Moreover, the shape of the GMR curve presents a parabolic variation around zero field, which is a good indication of better interlayer coupling than for the case with the Fe buffer [14]. This means that the magnetization vectors of the adjacent Co layers are fully antiparallel and follow a small angular variation for small applied magnetic fields. In addition, the Cr/Fe/Cu buffer contributes less to the sample total magnetic moment as compared to the usual 6 nm Fe buffer. The magnetic layer of the buffer stack constitutes a disadvantage for the analysis of the magnetic behavior of the antiferromagnetic sandwich. On the other hand, it provides a useful tool for testing the completeness of the antiparallel alignment of the Co layers at $H = 0$. This has been done [12] previously using different buffers. Thin magnetic layers of 0.8 nm Co and 1.8 nm $Ni_{80}Fe_{20}$ have been inserted between the 3 nm Fe layer and the 10 nm Cu layer. The analysis of the magnetoresistance curves around $H = 0$ and particularly the contribution to the GMR of the magnetic part of the buffer layer, when it switched after reversing the applied magnetic field, have shown that the remanence of the AF sandwich is negligibly small. Since there is no in-plane magnetic anisotropy in our sandwiches, the absence of the remanence is a good indication that the antiferromagnetic alignment is perfect and as a consequence the coupling is perfect.

These results have clearly shown that using appropriate growth conditions and optimal choice of the different layers, which constitute the buffer, we can obtain a strong AF coupling strength and a complete AF alignment at $H = 0$ and a large GMR. In the next part, structural analysis are developed in order to understand the physical mechanism at the origin of the optimized AF coupling and GMR.

4 Structural investigations

To characterize the physical parameters at the origin of the observed difference in the magneto-transport properties between the different buffers, two of them have been selected for the structural analysis. The Cr(4 nm)/Co(0.8 nm)/Fe(3 nm)/Cu(10 nm) buffer, which gives the best AF coupling and GMR, and the Cr(6 nm)/Co(0.8 nm)/Cu(10 nm) for which the coupling vanishes and the GMR is strongly reduced. These buffers have been analyzed by X-ray Diffraction, atomic force microscopy and transmission electron microscopy (TEM). For the B type buffer, the structural analysis has shown similar characteristics to the C type buffer, which explains the similarity between their magnetotransport properties.

4.1 X-ray diffraction

Figure 4 shows the high angle X-ray spectrum obtained for the Co(1.2 nm)/Cu(0.84 nm)/Co(1.2 nm) sandwich

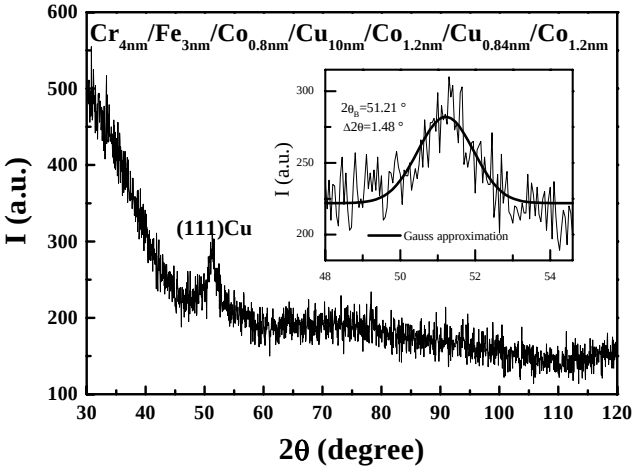

Fig. 4. High angle X-ray spectrum recorded at room temperature for the sandwich: Cr(4 nm)/Fe(3 nm)/Co(0.8 nm)/Cu(10 nm)/Co(1.2 nm)/Cu(0.84 nm)/Co(1.2 nm) using the Co kα_1 ($\lambda = 0.1789$ nm) wavelength.

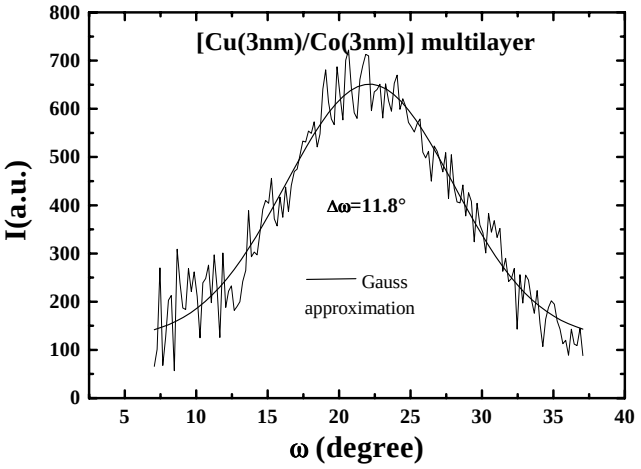

Fig. 5. Rocking curve performed on the Cu/Co multilayer deposited on C type buffer: Cr(4 nm)/Fe(3 nm)/Co(0.8 nm)/Cu(10 nm).

deposited on Cr(4 nm)/Fe(3 nm)/Co(0.8 nm)/Cu(10 nm) buffer. This experiment has been performed in the reflection mode. Only one Bragg peak is observed around $2\theta = 51°$. This peak is mainly the result of the 10 nm Cu decoupling layer since the other layers are too thin to contribute to the signal. Using the Bragg angle and the wavelength values, we find the average parameter $d_0 = 0.205$ nm, which corresponds to fcc structure with (111) texture along the growth direction. From the full width at the half maximum (FWHM), we obtain the coherence length along the growth direction $L\perp = 7.2$ nm. This is an indication of the size of the crystallites, which contribute to the diffraction. To confirm the observed texture, we have grown a $[\text{Cu(3 nm)/Co(3 nm)}]_{20}$ multilayer on the same substrate. The results are similar, with only one well resolved Bragg peak observed at the same angular position. These results give an indication that there is a preferential growth orientation along the (111) direction. However it does not constitute an absolute proof of the existence of the unique (111) texture because it corresponds to the strongest diffraction peak that we can detect on a fcc polycrystalline powder. Moreover, the rocking curve performed on the multilayer shows FWHM, $\Delta\omega$ of about 12° (Fig. 5). This large value is a good indication that the layers are not perfectly textured as will be confirmed by transmission electron microscopy.

Figure 6 shows the high angle X-ray spectrum obtained for the following sandwich: Cr(6 nm)/Co(0.8 nm)/Cu(10 nm)/Rh(2 nm)/Cr(12 nm). Rh gives a well defined contrast with Cu, hence the 2 nm Rh layer has been deposited in order to identify the nature of the Cu surface by transmission electron microscopy. The figure shows two Bragg peaks at $2\theta = 50.6°$ and $2\theta = 52.3°$ corresponding, respectively, to the fcc structure of Cu with (111) texture and the bcc structure of Cr with (110) texture. Such a result is not surprising, since it is well known that for the

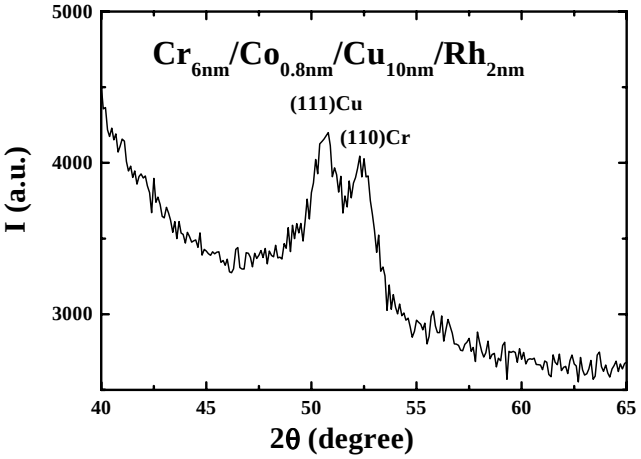

Fig. 6. High angle X-ray spectrum recorded at room temperature for the sandwich: Cr(6 nm)/Co(0.8 nm)/Cu(10 nm)/Rh(2 nm)/Cr(12 nm) using the Co kα_1 ($\lambda = 0.1789$ nm) wavelength.

Cr with bcc (110) texture, the epitaxial relationship is in favor of fcc Cu with (111) texture.

On the basis of the X-ray diffraction spectra, it is clearly seen that both Fe/Cr and Cr buffers stabilize the fcc structure of Cu with a slight (111) preferential texture. Thus, the difference in the magneto-transport properties cannot be attributed to the difference in the texture of the different buffers. This conclusion has to be carefully considered, since we know that the X-ray diffraction in $\theta/2\theta$ mode does not constitute an absolute proof of the observed texture. For this reason, these samples have to be analyzed by transmission electron microscopy in order to confirm the previous observation.

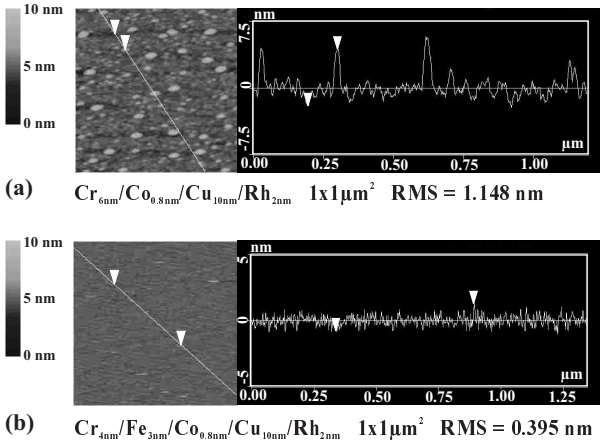

Fig. 7. Atomic force microscopy scan images performed on Cr(6 nm)/Co(0.8 nm)/Cu(10 nm)/Rh(2 nm) and Fe(4 nm)/Cr(3 nm)/Co(0.8 nm)/Cu(10 nm)/Rh(2 nm) buffers. The topography and the section analysis were performed on 1×1 μm^2 surfaces.

4.2 Atomic force microscopy

In order to understand the physical origin of the difference in the exchange coupling and the GMR, atomic force microscopy study have been performed on the Cr and Fe/Cr buffers with the following structure: Cr(6 nm)/Co(0.8 nm)/Cu(10 nm)/Rh(2 nm) and Fe(4 nm)/Cr(3 nm)/Co(0.8 nm)/Cu(10 nm)/Rh(2 nm). This technique will bring some information on the roughness of the buffer layers. The 2 nm Rh capping layer was used to protect the Cu layer against oxidation. Scans were made on 1×1 μm^2, and at different positions on the samples in order to have an average roughness value and to test the homogeneity of the surface. The distribution of the tip position on the vertical axis has been analyzed to obtain the average roughness. The tip-surface distance distributions are very well fitted by a Gaussian function, and the full width at the half maximum (RMS) values obtained for different scans are very similar, with a discrepancy between the values never exceeding 15%. This is a first indication that our surfaces are homogeneous. Figure 7 presents the topography of the two samples using surface 1×1 μm^2 area. The average RMS values are about 1.16 nm and 0.35 nm, respectively for Cr and Fe/Cr buffers, which means that the average roughness is very different between the two buffers. Thus, the surface of Fe/Cr/Co/Cu buffer is relatively flat with very localized islands, which is in favor of a nice antiferromagnetic coupling. This is a direct experimental evidence of the difference in the buffer surface roughness between the two buffers, which is at the origin of the difference in the magneto-transport properties. Indeed, as already reported for Co/Cu system, the exchange coupling oscillates between ferromagnetic and antiferromagnetic coupling over a thickness range of the Cu interlayer of typically 0.5 nm. In other words, the antiferromagnetic coupling only exists in a Cu-thickness window with a width smaller than 1 nm for an ideal interlayer with uniform thickness. This thickness window with perfect antiferromagnetic coupling, shrinks when the Cu thickness varies laterally. For large characteristic lengths of these variations, the maximum coupling strength and the saturation field remain unaffected, while the AF-coupling strength reduces at lengths that are small as compared to the lateral coherence length of the magnetization vector. This is exactly what happens in the case of the Cr buffer where the average roughness is of the same order as the oscillation period. Therefore, the average interlayer exchange coupling is mainly ferromagnetic with a small antiferromagnetic component and explains well the strong decrease of the exchange coupling strength. Moreover, since the GMR is directly related to the amount of the antiparallel alignment between the magnetization vectors of the adjacent Co layers, the GMR is strongly decreased in this case, as shown in the GMR curve. However, for the Fe/Cr buffer the average roughness is around 0.35 nm, which leads to spacer Cu thicknesses with mainly antiferromagnetic exchange coupling, and therefore, explains the high exchange coupling strength and the large GMR value observed for the sandwich deposited on the Fe/Cr buffer type.

4.3 Transmission electron microscopy

High Resolution Transmission Electron Microscopy (HRTEM) allows the direct observation of atomic-scale details of crystalline interfaces. This technique will bring some information on the effect of the buffer layer and its roughness on the coupling and GMR. First of all, a cross-section has been performed on a AAF sandwich deposited on the buffer similar to the C type buffer in order to confirm the (111) texture as suggested by X-ray diffraction (see Fig. 4). The thickness of the different layers of this sample *i.e.*, Cr(4 nm)/Fe(6 nm)/Cu(5 nm)/Co(5 nm)/Cu(5 nm)/Co(5 nm)/Cr(4 nm) has been chosen in order to perform easily optical diffractograms (Fig. 8). There is almost no Z-contrast between Cr, Fe and Cu, due to their close scattering potential values. In this case we have used the thickness of the different layers as determined by Electron Spectroscopy Imaging to determine the interfaces. The optical diffractogram of the Cu and Fe/Cr layers of the buffer reported in Figure 8 clearly shows the fcc (111) and bcc (110) respectively as growth direction. Nevertheless, the (100) growth direction for both layers has also been observed as shown in the Figure 8. This is a proof that the fcc (111) direction is not the unique growth direction.

Two other sandwiches used for the HRTEM cross-section have been especially chosen in order to make the understanding of the HRTEM images easier. They correspond to C and A types buffers with the following structures: Cr(4 nm)/Fe(3 nm)/Co(0.8 nm)/Cu(10 nm)/Rh(2 nm)/Cr(12 nm) and Cr(6 nm)/Co(0.8 nm)/Cu(10 nm)/Rh(2 nm)/Cr(12 nm). The 2 nm

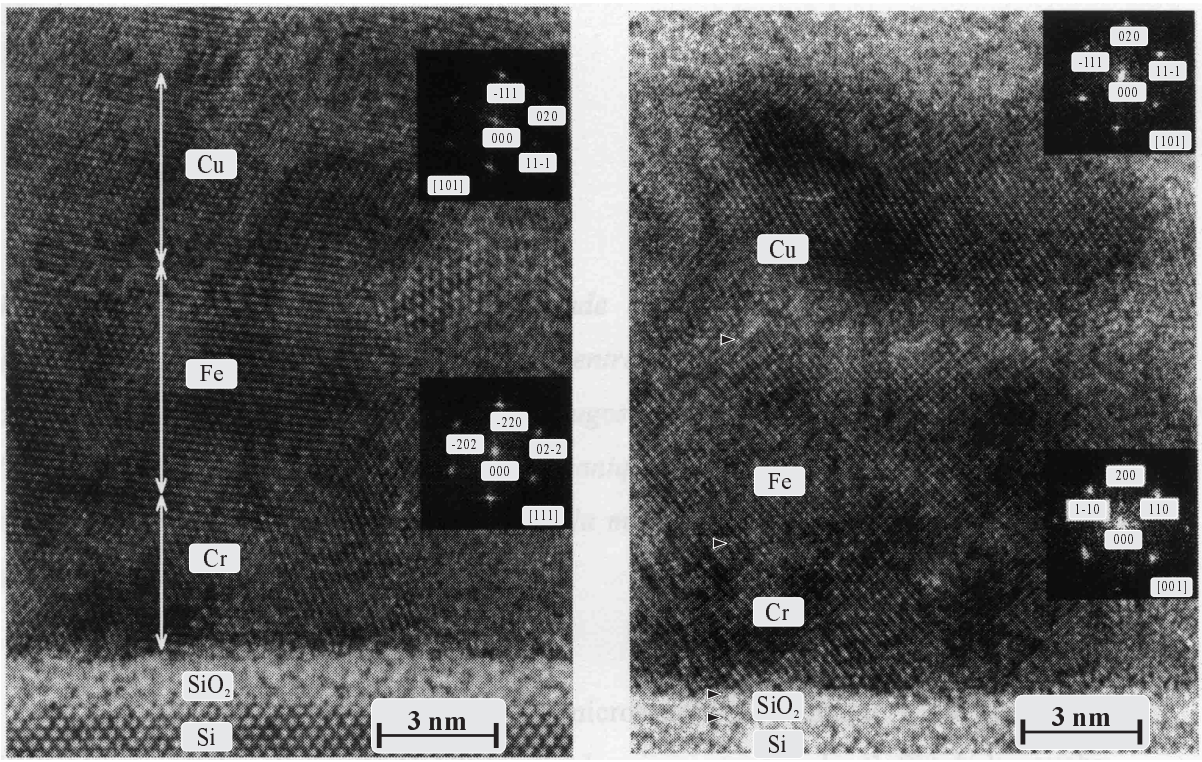

Fig. 8. Cross-sectional HRTEM pictures and their optical diffractograms for the C type buffer: Cr(4 nm)/Fe(3 nm)/Co(0.8 nm)/Cu(10 nm) sandwiches for: (a) with (111) Cu growth direction and (b) (100) Cu growth direction.

thin Rh layer has been deposited onto the Cu to highlight the roughness at the Cu surface, thanks to strong Z-contrast between Rh and Cu. On the other hand the 12 nm Cr layer has been deposited onto the Rh layer to protect the Cu/Rh interface during the mechanical milling. It also allows a better Cu/Rh interface resolution as compared to an uncovered layer, close to the glue used for cross-section processing.

Figure 9 shows the HRTEM cross-sectional images obtained for both sandwiches. These images clearly show the difference in the Cu surface roughness between the two buffers. The roughness of the Cu surface is more pronounced in the case of the Cr buffer (type A) than in the case of Cr/Fe buffer (type C). From these images we extract an average roughness values, which correspond to 0.3 and 1.2 nm, respectively for the Fe/Cr and the Cr buffers. These values are in good agreement with those determined by atomic force microscopy.

In order to have precise information on the texture between these two buffers and also on the size of the Cu grains, plan-view diffraction has also been performed on both samples and their Selected Area Diffraction (SAD) patterns are reported in Figure 10. The ring diffraction patterns suggest that both samples are polycrystalline giving rise to the same diffraction planes. To support the polycrystalline character of our samples, we have slightly tilted the electron beam by about 10° with respect to the growth direction. The results are exactly the same

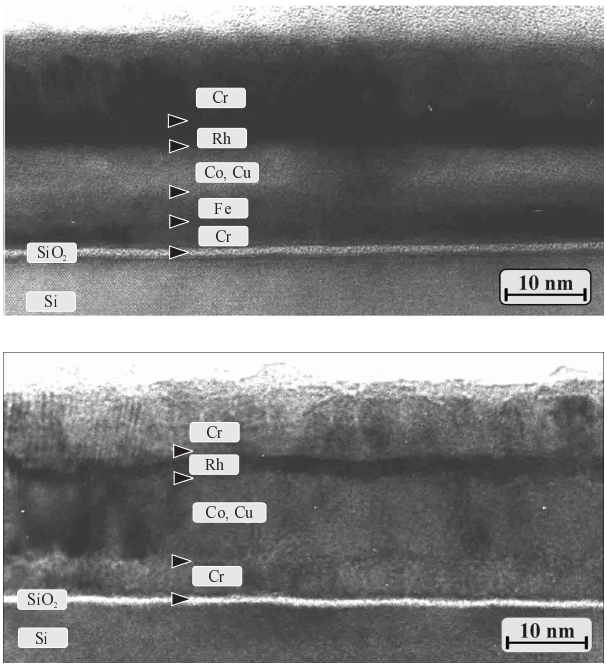

Fig. 9. Cross-sectional HRTEM images of (a) C type buffer: Cr(4 nm)/Fe(3 nm)/Co(0.8 nm)/Cu(10 nm)/Rh(2 nm)/Cr(12 nm) and (b) A type buffer: Cr(6 nm)/Co(0.8 nm)/Cu(10 nm)/Rh(2 nm)/Cr(12 nm) deposited on silicon substrates.

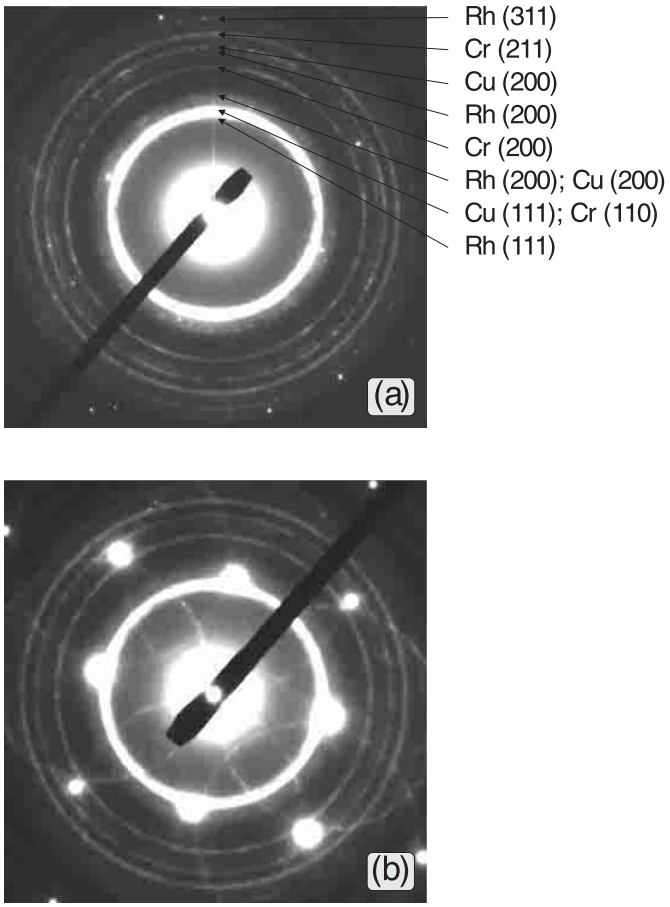

Fig. 10. TEM planar selected area diffraction patterns for: (a) C type buffer Cr(4 nm)/Fe(3 nm)/Co(0.8 nm)/Cu(10 nm)/Rh(2 nm)/Cr(12 nm) and (b) A type buffer: Cr(6 nm)/Co(0.8 nm)/Cu(10 nm)/Rh(2 nm)/Cr(12 nm) deposited on silicon substrates. The rings are compared to the expected radii for the diffraction Bragg peaks of Cu and Fe.

with the strongest ring corresponding to the fcc (111) Cu and the bcc (110)Cr/Fe, and confirm our hypothesis that there is no well defined preferential texture for both samples that can be observed in this geometry. However, the presence of the (111) diffraction peak is not surprising since the FWHM of the rocking curve around the (111) Cu diffraction peak is of about 12°. This corresponds mainly to the large angular distribution of the (111) Cu grains around the normal to the film and not to the grain sizes, which are of the order of 30 nm as determined by dark field images.

The structural analysis has shown that there is no clear difference in the crystalline character between the Cr and Fe/Cr buffers. Both give rise to a polycrystalline Cu layer with a slight texture along the (111) direction. However atomic force microscopy and transmission electron microscopy have clearly evidenced a strong difference in the average roughness between these two buffers.

5 Conclusion

To conclude, this work allows us to show a direct correlation between surface roughness and magneto-transport properties. The best giant magnetoresistance and the largest antiferromagnetic coupling strength for the Co/Cu/Co AAF sandwich have been obtained using the Cr/Co/Fe/Cu buffer which gives a smaller Cu surface roughness around 0.35 nm. X-ray diffraction and Transmission Electron Microscopy results show no sensitive difference in the crystalline quality and the preferential growth texture between the buffers, which exclude this hypothesis as a possible origin for the difference in the magneto-transport properties.

References

1. P. Grünberg, R. Schreiber, Y. Pang, M.B. Brodsky, H. Sowers, Phys. Rev. Lett. **57**, 2442 (1986).
2. M.N. Baibich, J.M. Broto, A. Fert, F. Nguyen van Dau, F. Petroff, P. Etienne, G. Creuzet, A. Friederich, J. Chazelas, Phys. Rev. Lett. **61**, 2472 (1988).
3. S.S.P. Parkin, R. Bhadra, K.P. Roche, Phys. Rev. Lett. **66**, 2152 (1991).
4. D.H. Mosca, F. Petroff, A. Fert, P.A. Schroeder, W.P. Pratt Jr, R. Laloe, J. Magn. Magn. Mater. **94**, L1 (1991).
5. W.F. Egelhoff Jr, M.T. Kief, Phys. Rev. B. **45**, 7795 (1992).
6. D. Greig, M.J. Hall, C. Hammond, B.J. Hickey, H.P. Ho, M.A. Howson, M.J. Walker, N. Wiser, D.G. Wright, J. Magn. Magn. Mater. **110**, L239 (1992).
7. M.T. Johnson, S.T. Purcell, N.W.E. McGee, R. Coehoorn, J. aan de Stegge, W. Hoving, Phys. Rev. Lett. **68**, 2688 (1992).
8. M.T. Johnson, R. Coehoorn, J.J. de Vries, N.W.E. McGee, J. aan de Stegge, P.J.H. Bloemen, Phys. Rev. Lett. **69**, 969 (1992).
9. A. Schreyer, K. Bröhl, J.F. Anker, C.F. Majkrzak, Th. Zeidler, P. Bödeker, N. Metoki, H. Zabel, Phys. Rev. B. **47**, 15334 (1993).
10. C. Dupas, E. Kolb, K. Le Dang, J.P. Renard, P. Veillet, E. Vélu, D. Renard, J. Magn. Magn. Mater. **128**, 361 (1993).
11. N. Persat, A. Dinia, J.P. Jay, C. Mény, P. Panissod, J. Magn. Magn. Mater. **164**, 37 (1996).
12. G. Rupp, K. Schuster, J. Magn. Magn. Mater. **121**, 416 (1993); H.A.M. van den Berg, *Fundamentals, Analysis and Industrial Application*, edited by U. Hartmann (Springer Verlag, Berlin, 1999), pp. 179–262.
13. N. Persat, H.A.M. van den Berg, A. Dinia, J. Magn. Magn. Mater. **165**, 446 (1997).
14. N. Persat, H.A.M. van den Berg, K. Cherifi-Khodjaoui, A. Dinia, J. Appl. Phys. **81**, 4748 (1997); N. Persat, H.A.M. van den Berg, A. Dinia, Phys. Rev. B. **62**, 3917 (2000).
15. S. Schmeuber, A. Hubert, G. Rupp, J. Magn. Magn. Mater. **166**, 267 (1997).
16. G. Rupp, H.A.M. van den Berg, IEEE Trans. Magn. **29**, 3102 (1993).
17. J. Benedict, R. Anderson, S.J. Klepeis, Mater. Res. Soc. Proced. **254**, 121 (1992).